Direct Observation in the Millisecond Time Range of Fluorescent Molecule Asymmetrical Interaction with the Electropermeabilized Cell Membrane

B. Gabriel and J. Teissié
Institut de Pharmacologie et de Biologie Structurale, Centre National de la Recherche Scientifique, UPR 9062, 31062 Toulouse, France

ABSTRACT Interaction of two stains (propidium iodide and ethidium bromide) with electropermeabilized living Chinese hamster ovary cells is observed using an ultrafast fluorescence image acquisition system. The computing process is linked to an ultra-low-light intensifying camera working with a very short time resolution (3.33 ms per image). Altered parts of the cell membrane were identified via the enhancement in fluorescence intensity of the dyes. They reflect the electropermeabilized part of the membrane in which free flow of dye occurred. Images of the fluorescence interaction patterns of the two dyes, in a maximum 20-ms time lag after pulsation, reveal asymmetrical permeabilization of the cell membrane. For electric field intensities higher than a first threshold value, permeabilization is always observed on the anode-facing side of the cell. For electric field intensities over a second higher threshold value, the two electrode-facing hemispheres of the cell are permeabilized, the hemisphere facing the anode being most permeable. These data support the conclusion that electropermeabilization of living cell membrane is affected by its resting potential. The asymmetrical pattern of the dye interaction is not dependent on the nature or concentration of the dye, the ionic strength of the pulsing buffer, or the duration of the pulse. The field intensity determines the fraction of the membrane in which molecular alterations can occur. The extent of alteration in this localized region is determined by the duration of the pulse when a single pulse in the millisecond time range is applied.

INTRODUCTION

Application of intense electric field pulses to living cells (electropulsation) allows a modulation of the electric potential difference across the membrane. The most dramatic consequence of the electric treatment is the reversible permeabilization of the cell membrane (electropermeabilization). The electroinduced high permeability allows the manipulation of the cell contents, such as the introduction of exogenous DNA into the cell (electrotransformation). An associated property of the membrane of electropermeabilized cells is fusogenicity. When electropermeabilized cells are brought into close contact, they fuse (electrofusion). Despite the widespread use of electropulsation in biology, the physical and structural bases of membrane destabilization remain unclear.

During pulsation, an electroinduced transmembrane potential difference ($\Delta\psi_i$) is created that is locally associated with the dielectric properties of the plasma membrane (Sale and Hamilton, 1968). Using a physical model based on a thin, weakly conductive shell full of an internal conductive medium and immersed in an external conductive medium, Laplace's equation describes $\Delta\psi_i$ as dependent on cell parameters and on the position on the cell surface (Kinosita and Tsong, 1977; Neumann, 1989):

$$\Delta\psi_i(M, E, t) = fg(\lambda)rE\cos[\theta(M)](1 - e^{-t/\tau_m}) \quad (1)$$

where M is the point on the cell we are considering, t is the time lag after electropulsation is turned on, f is a factor depending on the cell geometry (for a sphere, f is equal to 1.5) (Bernhardt and Pauly, 1973), r is the radius of the pulsed cell, $\theta(M)$ is the angle between the direction of the field and the normal of the cell surface, E is the electric field intensity, τ_m is the characteristic time constant of the membrane charge (in the microsecond time range) (Kinosita and Tsong, 1977; Ehrenberg et al., 1987), and $g(\lambda)$ is a function controlled by electric permeabilities (Gross, 1988; Neumann, 1989; Cartee and Plonsey, 1992).

The geometrical and kinetic dependence of $\Delta\psi_i$ was experimentally demonstrated in single cells by the use of potential sensitive electrochromic dyes (Gross et al., 1986; Kinosita et al., 1988). The electroinduced transmembrane potential difference is added to the resting one ($\Delta\psi_n$). When the new transmembrane potential difference ($|\Delta\psi_n + \Delta\psi_i|$) reaches a critical value ($\Delta\psi_c$) locally, an alteration of the membrane structure leads to reversible membrane permeabilization (electropermeabilization). As shown in Eq. 1, it is a local effect controlled by the field strength. $\Delta\psi_c$ was historically assumed to be ~1 V (Benz et al., 1979), but lower values for this threshold were reported (200–500 mV) for both model systems (Teissié and Tsong, 1981; Robello and Gliozzi, 1989) and living cells (Tomov and Tsoneva, 1989; Marszalek et al., 1990; Teissié and Rols, 1993).

The pulse-induced local perturbation of the membrane structure is in the micromillisecond time range. Therefore analysis of the electropermeabilization processes requires

Received for publication 28 May 1997 and in final form 4 August 1997.

Address reprint requests to Dr. Justin Teissié, Institut de Pharmacologie et de Biologie Structurale, Centre National de la Recherche Scientifique (UPR 9062), 118 route de Narbonne, 31062 Toulouse cédex 4, France. Tel.: 33-5-61-33-58-80; Fax: 33-5-61-33-58-60; E-mail: justin@lptf.biotoul.fr.

0006-3495/97/11/2630/08 $2.00

work at the membrane level of single cells, with high temporal and spatial resolution.

Previous investigations (Tekle et al., 1990; Teissié and Rols, 1993) indicated that the resting potential difference ($\Delta\psi_n$) is added to the electroinduced one and thus might be responsible for an asymmetrical permeabilization process. Such asymmetrical electropermeabilization has been observed after the pulse treatment, with different cell types, but the opposite results were reported. Entry of external molecules was predominately found on the positive electrode-facing cell side (Rossignol et al., 1983; Mehrle et al., 1985; Tekle et al., 1991, 1994; Djuzenova et al., 1996), whereas in the case of efflux of preloaded molecules (Sowers and Lieber, 1986) or in the case of sea urchin eggs (Kinosita et al., 1991, 1992), transport was mostly observed on the negative electrode-facing side. Furthermore, induced permeability observed during a microsecond pulse was reported as symmetrical (Hibino et al., 1991, 1993). In the latter case, electropermeabilization of sea urchin eggs was detected by submicrosecond imaging of the changes in transmembrane potential, and results were discussed, assuming that $\Delta\psi_c \approx 1$ V and $\Delta\psi_n = 0$ (Hibino et al., 1993).

More recently, Tekle et al. (1994) showed that a selective asymmetrical transport was observed across the electropermeabilized membrane. The authors suggested that this selectivity of the transport was based on the nature of the membrane electroinduced structure that supports this transport, and the transported molecules. The video system was limited by its time resolution (33 ms/image), and transport patterns were observed ~100 ms (for calcium influx) and more than 300 ms (for fluorescent dyes transport) after the electric pulse. As they concluded, no data were available to indicate whether such selective asymmetry was present at earlier times.

In the present work, using an ultrarapid video system (3.33 ms/image), we show that such a selective transport is not present immediately (less than 20 ms) after the application of the electric field. In addition, use of fluorescence probes specific to the alterated membrane area allows us to experimentally clarify the processes of electropermeabilization.

MATERIALS AND METHODS

Chemicals

Propidium iodide (PI, MW 668.4) and ethidium bromide (EB, MW 394.3) were purchased from Sigma (St. Louis, MO). 2,5′-Bi-1H-Benzimidazole, 2′-(4-ethoxyphenyl)-5-(4-methyl-1-piperarinyl)-trihydrochloride (Hoechst 33342) was obtained from Molecular Probes (Eugene, OR). Standard isoosmotic pulsing buffer (PB) was 250 mM sucrose, 1 mM $MgCl_2$, and 10 mM potassium phosphate buffer (pH 7.4). Potassium-containing pulsing buffer (PBK) was 69 mM KCl, 125 mM sucrose, 1 mM $MgCl_2$, and 10 mM potassium phosphate buffer (pH 7.4). Conductivity and osmotic pressure were 1.5 mS/cm and 312 ± 3 mOs/kg for PB, and 7.1 mS/cm and 270 ± 2 mOs/kg for PBK.

Cell culture

Chinese hamster ovary (CHO) cells (WTT clone) were grown in suspension in completed Eagle's minimum essential medium (MEM 0111; Eurobio, Paris, France) to avoid trypsin treatment, as previously described (Gabriel and Teissié, 1995a).

Cell labeling with Hoechst 33342

The cells (10^6 cells/ml) were suspended in the staining solution (10 μM Hoechst 33342 in PB) for 30 min, at 21°C, under gentle agitation. After incubation, the labeled cells were washed and resuspended in dye containing buffer for electropermeabilization observation.

Cell electropermeabilization

Cells were harvested by centrifugation for 10 min at 100 × *g* (700 rpm, C500 centrifuge; Jouan, St. Herblain, France), washed, and resuspended in the appropriate dye containing pulsing buffer (10^6 cells/ml). A single square-wave electric pulse with desired parameters (voltage and duration) was supplied by a CNRS electropulser (Jouan). Pulse parameters were monitored through a 15-MHz oscilloscope (Enertec, St. Etienne, France). A special electropulsation chamber was built with two stainless steel parallel rods (diameter 0.5 mm, length 10 mm) stuck on a 22 × 32 mm microscope glass coverslip. The interelectrode distance was 5 mm. The chamber was installed under the inverted digitized videomicroscope. A 70-μl cell suspension that contained indicating dye was placed between the electrodes. A 2-min time lag was allowed for cell sedimentation on the coverslip surface. The electric pulse was applied and fluorescence images of the electropulsed cell were then recorded with a maximum 20-ms time lag after the end of the pulse.

Fluorescence image acquisition and processing

Our ultrarapid fluorescence image acquisition system is detailed in Fig. 1. Cells in the electropulsation chamber were observed by fluorescence under the oil immersion objective (magnitude 63 Leitz objective; Leitz, Wetzlar, Germany) of a Leitz inverted microscope. The light source was an HBO 100W2 lamp (Osram, Munich, Germany). When PI and EB were used, the wavelengths were selected with a Leitz N2 filter block (530 nm ≤ λ_{exc} ≤ 560 nm; 580 nm ≤ λ_{em}). For Hoechst 33342-labeled cells, the Leitz A filter block was used (340 nm ≤ λ_{exc} ≤ 380 nm; 430 nm ≤ λ_{em}). A video monitoring set up was connected to the microscope: a rapid ultra-low-light intensifying camera (LH 750-ULL rapid; Lhesa, Cergy-Pontoise, France)

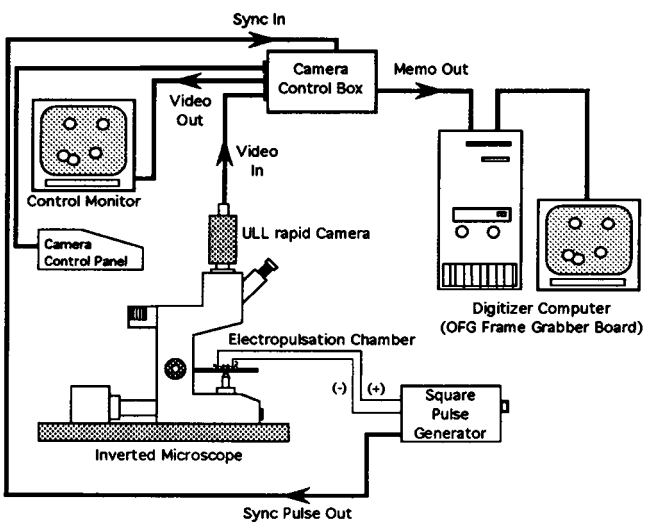

FIGURE 1 Schematic drawing of the fluorescence microscope, and image acquisition and electropermeabilization apparatus (see Materials and Methods). Arrows represent signal directions (TTL and video).

associated with a color monitor (Trinitron; Sony, Fellbach, Germany). The camera allowed real-time fluorescence acquisition with a 300-Hz frequency (3.33 ms/image). The fluorescence pattern of the dye immediately after electropulsation (less than 20 ms) was recorded in the memory board of the camera control box. Two simultaneous 20-ms video frames were stored that represented 12 consecutive 3.33-ms images. The images were then transferred to a PC computer (AT/486) by using a frame grabber board (IP8; Matrox, Québec, Canada). The video signal was converted to a numerical matrix with 8-bit grey scale, that is, 256 different light levels. The size of the matrix was 512 × 576. Acquisition and image processing were obtained with Optimas 4.02 software (Bioscan, Edmonds, WA). The rising edge of the TTL signal associated with the electric square pulse was used to trigger the memorization of two successive frames (i.e., 40 ms). The gain of the camera was fixed by manual adjustment. Thus the light levels were directly comparable between images. Mathematical processing was as previously described (Gabriel and Teissié, 1995b). Briefly, the blank image (fluorescence image of the cell before electropulsation) was subtracted from the image of the transport pattern observed in the same cell after electropulsation to allow correction of the background. No other mathematical treatment was used.

THEORY

Taking into account the interaction of the negative resting transmembrane potential difference $\Delta\psi_n$ with the electroinduced one $\Delta\psi_i$, electropermeabilization may occur for lower electric field intensities on the anode-facing hemisphere (positive electrode), and only for higher field intensities on the cathode-facing hemisphere (negative electrode) of the pulsed cell (Tekle et al., 1990; Teissié and Rols, 1993). From Eq. 1 it is possible to define two threshold values of electric intensity, E_p and E_f, for the anode side ($\theta = 0$) and the cathode side ($\theta = \pi$), respectively, as

$$E_p = (\Delta\psi_c - \Delta\psi_n)/fg(\lambda)r \quad (2)$$

$$E_f = (\Delta\psi_c + \Delta\psi_n)/fg(\lambda)r \quad (3)$$

In other words, electropermeabilization is triggered on the anode-facing hemisphere when $E = E_p$, and on the cathode-facing hemisphere when $E = E_f$.

From a given electric field intensity E, it is possible from Eq. 1 to define the membrane area through which electropermeabilization-induced transport should occur, by the characteristic angles $\theta^a_{max}(E)$ (for the anode side, $0 \leq \theta^a_{max}(E) \leq \pi/2$) and $\theta^c_{max}(E)$ (for the cathode side, $\pi/2 \leq \theta^c_{max}(E) \leq \pi$), defined as follows:

when $E_p < E \leq E_f$

$$\cos[\theta^a_{max}(E)] = (\Delta\psi_c - \Delta\psi_n)/[fg(\lambda)rE] \quad (4)$$

when $E_f < E$

$$\cos[\theta^a_{max}(E)] = (\Delta\psi_c - \Delta\psi_n)/[fg(\lambda)rE] \quad (5)$$

$$|\cos[\theta^c_{max}(E)]| = (\Delta\psi_c + \Delta\psi_n)/[fg(\lambda)rE]$$

Equations 4 and 5 show that the dimension of the membrane area that is electropermeabilized depends on the reciprocal of the field intensity. Previous quantitative analysis of electropermeabilization of CHO cells showed that the electropermeabilized part of the membrane was more accurately related to $(1 - E_p/E)$ (Rols and Teissié, 1990).

Alternatively, symmetrical electroporation has been proposed (Hibino et al., 1991). The authors suggested that "poration on only one side of the cell will immediatly double the membrane potential on the opposite side," and therefore trigger "immediate poration of this side."

RESULTS

Interaction of the fluorescent dye with the electropermeabilized cell

Electropermeabilization of CHO cells in suspension was monitored by using PI and EB, which are both naturally relatively membrane impermeant (Sixou and Teissié, 1993). Fig. 2 shows that interaction of PI with an electropermeabilized cell in the millisecond after electropulsation could be visualized by the area at the cell periphery with enhanced fluorescence. This peripherical fluorescence was not due to the binding of PI to the nucleus DNA. Fig. 2 *A* shows a CHO cell in metaphase, as shown by the Hoechst labeling (Fig. 2 *B*). Although nucleus DNA was condensed in the equatorial plate in the center of the cell, a well-defined peripheral area with enhanced PI fluorescence has been observed (Fig. 2 *C*). This fluorescent area was facing the anode. The shape and the localization of this fluorescence pattern appeared to be characteristic of membrane labeling

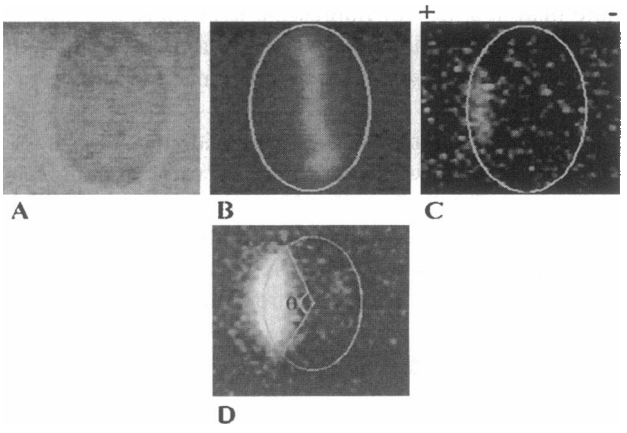

FIGURE 2 Video frames showing the localization in electropermeabilized CHO cells of the fluorescence associated with PI. Electropermeabilization is achieved in PB, and the dye used is PI (1 mM). The position of the electrodes is as shown: positive (anode) to the left and negative (cathode) to the right of the frame. (*A*) Phase-contrast image of the cell before electric pulse and previously labeled with Hoechst 33342. Radius = 6.5 μm. (*B*) The same cell viewed in fluorescence mode, showing Hoechst staining of DNA. The observed labeling is characteristic of a CHO cell in metaphase. (*C*) The same cell viewed in PI fluorescence mode, after electropermeabilization (one 20-ms pulse of 600 V/cm). The localized enhanced peripheral fluorescence indicates the entry site of PI across the plasma membrane. (*D*) Determination of the experimental characteristic angle $\theta^a_{exp}(E)$. Fluorescence levels are mathematically amplified threefold. The CHO cell is observed in PI-fluorescence mode less than 20 ms after electropermeabilization using one 20-ms pulse of 700 V/cm.

(El Ouagari et al., 1993). The average gray level of this fluorescence crescent remained constant right through the total time of observation (40 ms, i.e., 12 successive images) (data not shown). A steady state of alteration was then present. It was then possible to graphically measure the polar angle $\theta(E)$ of the labeled part of the cell surface (Fig. 2 *D*). In this way we experimentaly obtained the angles $\theta^a_{exp}(E)$ and $\theta^c_{exp}(E)$, defined as the half of the polar angle of the fluorescent part of the anode- and cathode-facing sides, respectively. Such characteristic angles were defined for the different buffers (PB and PBK) and dyes (PI and EB) we used.

Dependency of the cell fluorescence labeling on the electric field intensity

Fig. 3 shows the dependency of the electropermeabilized dye fluorescence pattern on the electric field intensity. CHO cells in suspension were electropulsed in 1 mM PI-containing PB. Localized peripheral labeling occurred only when cells were electropulsed with electric field intensities higher than an apparent threshold value of ~500 V/cm (Fig. 3, *A* and *B*). This labeling always appeared on the anode-facing side of the cell. Above this threshold value, an increase in electric field intensity led to an increase in the dimensions of the peripheral labeled crescent present on the anode-facing side of the cell (Fig. 3, *B–F*). Maximum labeling of the cell was obtained when 1.2 kV/cm was applied (Fig. 3 *F*). Simultaneously, a cathode-facing hemisphere labeling was observed for electric field intensities higher than 700 V/cm (Fig. 3, *D–F*). As observed for the anode-facing side, increasing the field intensity above this value led to an increase in the dimensions of the labeled cell crescent. Similar results were obtained when EB was used as the dye (data not shown). The characteristic angles $\theta^a_{exp}(E)$ and $\theta^c_{exp}(E)$ depended on the electric field intensity. This dependency was reported in the case of $\theta^a_{exp}(E)$ as a function of the reciprocal of the field intensity ($1/E$) (Fig. 3 *G*). $1/E$ is linearly related to the part of cell membrane area that is globally electropermeabilized (Schwister and Deuticke, 1985; Rols and Teissié, 1990). Results show a linear fit between $\theta^a_{exp}(E)$ and the predicted electropermeabilized area. Extrapolation for $\theta^a_{exp}(E) = 0$ (i.e., $\cos[\theta^a_{exp}(E)] = 1$) allowed the determination of the critical threshold value of field intensity for permeabilization. From Fig. 3 *G*, we graphically found $E_p = 515 \pm 5$ V/cm. A similar linear fit was observed between $\theta^c_{exp}(E)$ and $1/E$, and the critical threshold value for cathode side permeabilization was $E_f = 750 \pm 15$ V/cm (data not shown). The average fluorescence level associated with the labeled cell surface depended on the electric field intensity (see Fig. 3, *B–F*). The dependency of the fluorescence on the field intensity was reported as a function of $(1 - E_p/E)$, which is directly representative of the extent of the electropermeabilized membrane area (Fig. 3 *H*) (Rols and Teissié, 1990; Gabriel, 1992). Results show a linear relationship between fluorescence level and electropermeabilized membrane area. The two dyes displayed similar behaviors when CHO cells were electropulsed in PBK. The results are summarized in Table 1. Data are reported for CHO cells with a radius equal to 6.5 μm. We

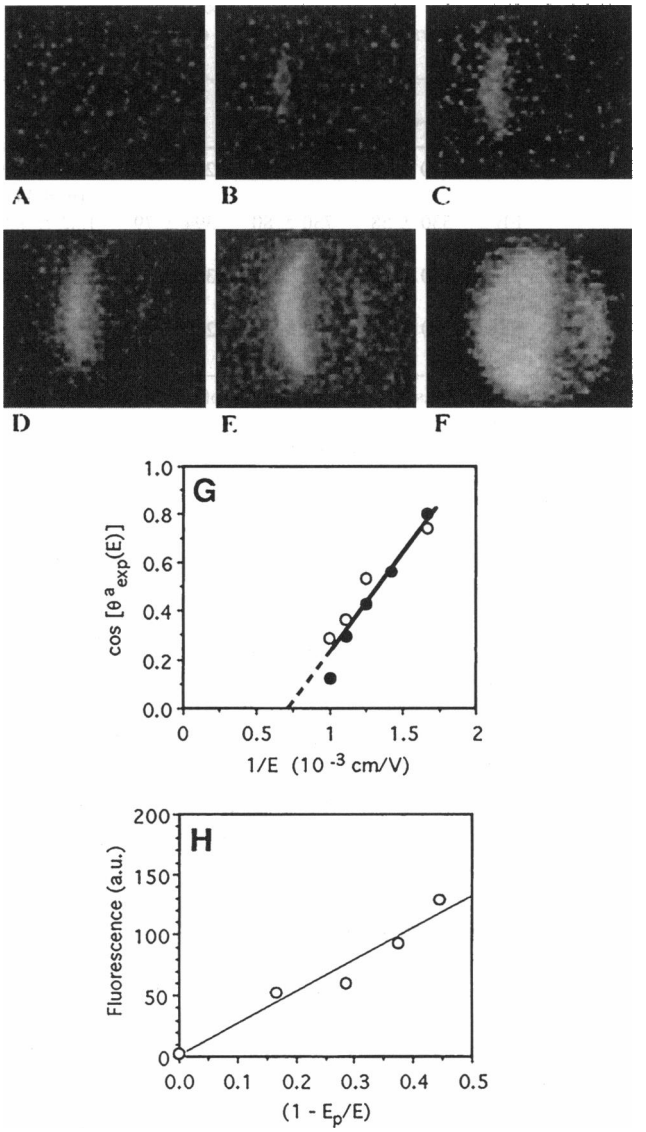

FIGURE 3 Selected video frames showing the fluorescence of PI associated with electropermeabilized CHO cells under different electrical conditions. (*A–F*) Cells were electropulsed in 1 mM PI containing PB, using one 20-ms pulse with increasing field intensities. They were observed less than 20 ms after pulsation. The positive electrode is on the left and the negative one on the right of each frame. (*A*) 500 V/cm. (*B*) 600 V/cm. (*C*) 700 V/cm. (*D*) 800 V/cm. (*E*) 900 V/cm. (*F*) 1200 V/cm. (*G*) Dependence of the characteristic angle $\theta^a_{exp}(E)$ on the reciprocal of the electric field intensity ($1/E$). Experimental conditions were one 20-ms pulse, and CHO cells were electropulsed in 1 mM PI (●) or 1 mM EB (○) containing PB. The correlation coefficient of the linear fit is equal to 0.93. (*G*) Relation between the membrane area extent electrically altered and the average fluorescence level of the peripheral labeled area observed after pulsation. Fluorescence levels are reported as a function of $(1 - E_p/E)$, with E_p equal to 515 V/cm. CHO cells were pulsed with one 20-ms pulse in 1 mM PI-containing PB. The correlation coefficient of the linear fit was found to be 0.95.

TABLE 1 Electrical parameters obtained from dependence of experimental characteristic angles on electric field intensities

Medium	Dye*	E_p (V/cm)	E_f (V/cm)	$\Delta\psi_c^{\#}$ (mV)	$f\,g(\lambda)^{\S}$
PB	PI	490 ± 54	750 ± 82	286 ± 57	0.90 ± 0.19 (n = 11)
	EB	530 ± 58	730 ± 80	394 ± 79	1.32 ± 0.20 (n = 13)
PBK	PI	560 ± 62	780 ± 85	365 ± 72	1.33 ± 0.42 (n = 16)
	EB	480 + 53	745 ± 82	277 ± 55	0.97 ± 0.22 (n = 13)

*Concentration used was 1 mM. The duration of the single pulse was 20 ms.

#Critical thresholds in transmembrane potential were obtained from equation 8 in Teissié and Rols (1993), using reported data in this table, and $|\Delta\psi_n| = 60$ mV.

§Calculations were obtained from Eqs. 4 and 5, using $\Delta\psi_c$ values reported in this table and graphically measured characteristic angles.

obtained fairly similar values for thresholds E_p and E_f in the two media. From data of Table 1, we obtained $E_p = 515 \pm 37$ V/cm and $E_f = 750 \pm 20$ V/cm. These two thresholds were the same for PI and EB. From equation 8 in Teissié and Rols (1993), the critical threshold in electrical transmembrane potential difference was calculated. No statistical difference was observed for $\Delta\psi_c$ values, whatever the medium and dye used. Average value obtained was equal to 330 ± 90 mV. The product $[f\,g(\lambda)]$ was nearly the same in the two buffers and for the two dyes we used. An average value of 1.07 ± 0.33 (sampling, n = 53) was found.

Effects of number and duration of electrical pulses

For a single pulse of 1.5 kV/cm with variable duration (from 240 μs to 3 ms), fluorescence enhancement was simultaneously observed on both sides of the cell (Fig. 4, *A–D*). The characteristic angles defined for the two sides ($\theta^a_{exp}(E)$ and $\theta^c_{exp}(E)$) did not depend on the duration of the pulse (Fig. 4 *E*). On the other hand, the average fluorescence level associated with the labeled cell surface depended on the duration (Fig. 4 *F*). Increasing the duration of the pulse resulted in an increase in the fluorescence level of the two cell side regions without any changes in their geometry. The average fluorescence level associated with the labeled area depended on the concentration of the dye (Fig. 4 *G*). The fluorescence intensity increased linearly when the concentration of dye was increased to 0.25 mM PI, and saturation was observed for higher concentrations. The characteristic angles ($\theta^a_{exp}(E)$ and $\theta^c_{exp}(E)$) did not depend on the concentration of dye (data not shown).

Long time-associated asymmetrical labeling

Fig. 5 shows the two types of fluorescence labeling of cells obtained 30 s after electropermeabilization in 0.1 mM PI-

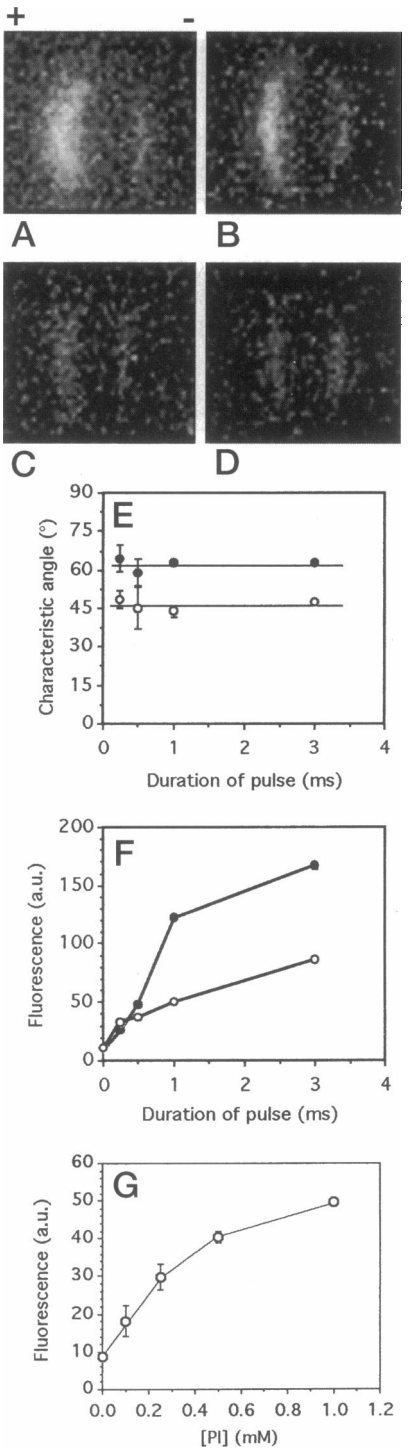

FIGURE 4 Effect of the duration of the pulse and of the concentration of dye on the fluorescence transport pattern. (*A–D*) Selected video frames showing the effect of the duration of the pulse on the fluorescence transport pattern. Experimental conditions were one single pulse of 1.5 kV/cm in 0.5 mM PI containing PB. The positive electrode is on the left and the negative one on the right of each frame. (*A*) 3 ms. (*B*) 1 ms. (*C*) 0.5 ms. (*D*) 0.24 ms. (*E*) Dependence of the electropermeabilized membrane area on the duration of the pulse. ●, Anode side; ○, cathode side. (*F*) Effect of the duration of the pulse on the average fluorescence level of the electropermeabilized membrane area. ●, Anode side; ○, cathode side. (*G*) Effect of the concentration of dye (PI). CHO cells were pulsed with one 20-ms pulse of 700 V/cm, in PI-containing PB.

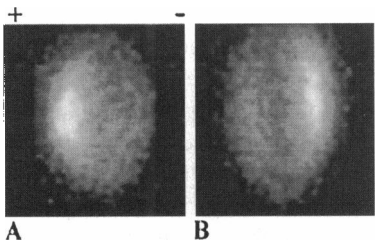

FIGURE 5 Selective transport pattern obtained a long time after electropermeabilization (30 s). CHO were electropermeabilized in 0.1 mM PI containing PB using one 20-ms pulse of 700 V/cm. The positive electrode is on the left and the negative one on the right of each frame. (*A*) Predominant labeling of the cytoplasmic region facing the anode (42 ± 7.5% of observations). (*B*) Predominant labeling of the cytoplasmic region facing the cathode (58 ± 7.5% of observations).

containing PB (electrical conditions: one 20-ms pulse of 700 V/cm). In both cases, the fluorescence enhancement obtained immediately after the electric field application was always only observed on the anode-facing side of the cell. Predominant labeling on the cell region facing the anode and the cathode represented, respectively, 42 ± 7.5% and 58 ± 7.5% of the observations (three experiments, i.e., 36 CHO cells).

DISCUSSION

PI and EB fluorescence spectra and quantum yields are highly environment-dependent. These two dyes are classically known as nucleic acid stains. Their fluorescence properties specifically allow observation of their entry into electropermeabilized cells (Sixou and Teissié, 1993; Tekle et al., 1994; Djuzenova et al., 1996). On the other hand, they were previously described as tools for the study of membrane mechanisms because of their change in fluorescence when bound to membrane loci (Gitler et al., 1969; Sator et al., 1977; Crosby et al., 1979). The increase in fluorescence quantum yield on binding to membrane reflects the immersion of the dye in a more structured and/or hydrophobic environment. Using these dyes and an ultrarapid and sensitive fluorescence acquisition system (3.33 ms per image), we visualize fluorescence-labeled regions associated with the electropermeabilized state of cells. The geometry of the labeled area on the cell suggests a membrane localization (Fig. 2, *A–C*). Kinetic analysis of the geometry and of the fluorescence level of labeled membrane areas shows that no change is observed at 40 ms (i.e., 12 successive images). A slowly increasing cytoplasmic labeling of the electropermeabilized cell is observed after longer times (Fig. 5). A transmembrane influx of the dye takes place that is associated with the permeabilized state of the membrane. As a continuous increase of fluorescence intensity would be expected if fluorescence were associated with a cytoplasmic binding of the dye to cellular targets (e.g., RNAs) (as indeed was previously observed; Sixou and Teissié, 1993), the stable and fast observed labeling appears to be the direct visualization of the dye interaction with the alterated (i.e., electropermeabilized) part of the membrane. Stability of the membrane fluorescence throughout 12 successive images indicates that a steady state of the molecule interaction with the membrane is achieved less than 20 ms after pulsation. Rather than binding of the dye to cytoplasmic nucleic acids closely localized to the membrane, the enhancement of fluorescence should be associated with a direct interaction of the dye with the membrane compounds (Gitler et al., 1969; Sator et al., 1977; Crosby et al., 1979). Our system allows clear determination of the membrane area in which electropermeabilization occurs. Characteristic experimental angles of the electropermeabilized membrane areas can therefore be graphically measured (Fig. 2 *D*). Our experimental measurements agree with the theory of asymmetrical electropermeabilization described by Eqs. 4 and 5.

Electropermeabilization is first triggered on the anode-facing pole of the cell when the electric field intensity applied is higher than a threshold value (E_p = 515 ± 37 V/cm for a CHO cell with a radius of 6.5 μm) (Fig. 3, *A–B*). For higher electric field intensities, the dimension of the permeabilized area increases, and electropermeabilization appears on the cathode-facing pole of the cell, only at E_f = 750 ± 21 V/cm for CHO cell with the same diameter (Fig. 3, *C–F*). E_p and E_f are different, as expected from the contribution of the resting membrane potential (Tekle et al., 1990; Teissié and Rols, 1993) (Eqs. 2 and 3). Our findings are different from those from sea urchin eggs, in which membrane conductance was measured during the pulse, for which the two sides facing the electrodes were almost equally permeabilized as soon as the field intensity was high enough to trigger permeabilization (Hibino et al., 1991, 1993). In this former work, the resting potential of egg membrane was neglected and $\Delta\psi_c$ was taken to be equal to 1 V.

The dimension of the permeabilized membrane region depends on the reciprocal of the field intensity (Fig. 3 *G*). Whatever the nature of the dye (PI or EB) and the ionic strength of the buffer (PB or PBK), dependency of asymmetrical transport patterns on electric field intensity is always the same (Fig. 3 *G* and data not shown). The two threshold values of field E_p and E_f do not depend on the molecule used to report transport (Table 1). As the size of the observed cell is kept the same, E_p and E_f values do not depend on the ionic strength of the pulsing buffer, as previously reported for CHO cells (Rols and Teissié, 1989). This contradicts recent statements of other authors that the threshold field intensity E_p for PI uptake in myeloma cells depends on ionic strength (Djuzenova et al., 1996). It was previously observed that E_f is classically 1.5–2 times E_p in the case of mammalian cells (Zimmermann and Vienken, 1984). A ratio of ~1.5 is found here for CHO cells. It is currently assumed that the resting potential difference of CHO cells is ~60 mV (Teissié and Rols, 1993), is constant all over the cell surface, and is centripetal. The experimental determination of $\Delta\psi_c$, obtained by direct observation of permeabilization on single cells (Table 1), confirms a much

smaller value than historically assumed. A value of 1 V was generally reported, whereas much smaller values were recently found (Teissié and Tsong, 1981; Robello and Gliozzi, 1989; Tomov and Tsoneva, 1989; Marszalek et al., 1990; Teissié and Rols, 1993). We show that $\Delta\psi_c$ does not depend on the ionic strength of the pulsing buffer (Table 1), or on the concentration of dye, or on the duration of the pulse (data not shown). Inserting $\Delta\psi_c$ into Eqs. 4 and 5, we obtain a statistical value of 1.07 ± 0.22 for the product $[f\,g(\lambda)]$ (53 cells) (Table 1). This parameter is classically assumed to be 1.5 when the cell membrane conductivity is presumed to be negligible. Here we demonstrate that for CHO cells in suspension, such a hypothesis is not justified.

Fig. 3 *H* shows that the average fluorescence of the labeled cell membrane depends linearly on the extent of the electropermeabilized area. Fluorescence is proportional to the steady-state interaction of the dye with the electropermeabilized part of the membrane. The linear fit obtained suggests that the interaction does not depend on the electric field intensity, as expected if any electrophoresis transport during the pulse were involved, as proposed by others (Dimitrov and Sowers, 1990; Prausnitz et al., 1995). Furthermore, Fig. 3 *H* also shows that the interaction of the dye is homogeneous all over the electropermeabilized part of the cell membrane, whatever its dimensions. The electroinduced interaction is directly related to the concentration of dye (Fig. 4 *G*) and depends on the duration of the pulse (Fig. 4, *A–D* and *F*). The electric field intensity defines the same electropermeabilized area, whatever the duration of the pulse (Fig. 4 *E*). We observe directly that duration of the pulse plays an important role in the process, in line with the previous observations that the duration of the pulse determines the density of structures that support the transport (Rols and Teissié, 1990), and that the membrane conductance was found to increase during the pulse (Hibino et al., 1993). Our data contradict the hypothesis of the simultaneous permeabilization of the two cell sides (Hibino et al., 1991), and they rule out the implication of field-associated, electrophoresis-induced transport, as previously believed.

Post-pulse asymmetrical events in electropermeabilized cells have previously been observed, but never with our time resolution (3.33 ms per image) and with probes at membrane level. The fastest observation of transport known to us was performed with 17-ms time resolution (Dimitrov and Sowers, 1990). Millisecond measurements of the electropermeabilization-induced transport were obtained by a photometric approach using a single calcein-loaded ghost (Prausnitz et al., 1995). However, no data were supplied about any preferential transport through electropermeabilized membrane areas. In this report, we show that immediately (less than 20 ms) after application of a pulse that triggers permeabilization of one side of the cell, an initial entry is observed exclusively through the anode-facing hemisphere of the cell, as also observed with sea urchin eggs (Rossignol et al., 1983), plant protoplasts (Mehrle et al., 1985), and National Institutes of Health 3T3 and CHO cells (Tekle et al., 1991, 1994). Results are the opposite of those obtained by other groups using erythrocyte ghosts (Sowers and Lieber, 1986) and sea urchin eggs (Kinosita et al., 1991, 1992). No selective transport is observed as previously reported for longer postpulsation times in CHO cells pretreated with trypsin (Tekle et al., 1994). Asymmetrical labeling was also observed here, but a long time after electropermeabilization (Fig. 5). The long time selectivity is not caused by electrophoresis as shown above, but can be explained by the binding of the dye to the nucleus DNA, the position of the nucleus in the cell being different.

To sum up, we have developed an ultrarapid video system that allows us, for the first time, to directly visualize the electropermeabilized part of the cell membrane and to give experimental bases for the understanding of the electropermeabilization process. Our results show that for a single CHO cell and using square-wave electric pulses, 1) permeabilization remains local on the cell surface, 2) the part of the cell membrane globally affected by the treatment depends on the electric field intensity, 3) the extent of permeability depends only on the duration of pulse, and 4) the molecular interaction of the dye with the local permeabilized membrane area depends on the concentration gradient of the molecule, as for free diffusion (Fick's law), and is homogeneous on the permeabilized area.

Thanks are due to Mss. M. C. Vernhes and M. Golzio, and to Dr. P. Demange for their comments, and to Mr. J. Robb for rereading the manuscript. Technical assistance was provided by the LHESA electronique and IMASYS companies.

This work was partly supported by grants from the Association pour la Recherche contre le Cancer and from the Ministère de la Recherche ACR "Physicochimie des membranes biologiques."

REFERENCES

Benz, R., F. Beckers, and U. Zimmermann. 1979. Reversible electrical breakdown of lipid bilayer membranes: a charge-pulse relaxation study. *J. Membr. Biol.* 48:181–204.

Bernhardt, J., and H. Pauly. 1973. On the generation of potential difference across the membrane of ellipsoidal cells in an alternating electric field. *Biophysik.* 10:89–98.

Cartee, A. L., and R. Plonsey. 1992. The transient subthreshold response of sperical and cylindrical cell models to extracellular stimulation. *IEEE Trans. Biomed. Eng.* 39:76–85.

Crosby, B., M. Boutry, and A. Goffeau. 1979. Inhibition of soluble yeast mitochondrial ATPase by ethidium-bromide. *Biochem. Biophys. Res. Commun.* 88:448–455.

Dimitrov, D. S., and A. E. Sowers. 1990. Membrane electroporation—fast molecular exchange by electroosmosis. *Biochim. Biophys. Acta.* 1022: 381–392.

Djuzenova, C. S., U. Zimmermann, H. Frank, V. L. Sukhorukov, E. Richter, and G. Fuhr. 1996. Effect of medium conductivity and composition on the uptake of propidium iodide into electropermeabilized myeloma cells. *Biochim. Biophys. Acta.* 1284:143–152.

Ehrenberg, B., D. L. Farkas, E. N. Fluhler, Z. Lojewska, and L. M. Loew. 1987. Membrane potential induced by external electric field pulses can be followed with a potentiometric dye. *Biophys. J.* 51:833–837.

El Ouagari, K., B. Gabriel, H. Benoist, and J. Teissié. 1993. Electric field-mediated glycophorin insertion in cell membrane is a localized event. *Biochim. Biophys. Acta.* 1151:105–109.

Gabriel, B. 1992. Electroperméabilisation de cellules de mammifères. Analyse des réponses cellulaires, en particulier du stress oxydatif. Ph.D thesis. Toulouse III.

Gabriel, B., and J. Teissié. 1995a. Control by electrical parameters of short- and long-term cell death resulting from electropermeabilization of Chinese hamster ovary cells. *Biochim. Biophys. Acta.* 1266:171–178.

Gabriel, B., and J. Teissié. 1995b. Spatial compartmentation and time resolution of photooxidation of a cell membrane probe in electropermeabilized Chinese hamster ovary cells. *Eur. J. Biochem.* 228:710–718.

Gitler, C., B. Rubalcava, and A. Caswell. 1969. Fluorescence changes of ethidium bromide on binding to erythrocyte and mitochondrial membranes. *Biochim. Biophys. Acta.* 193:479–481.

Gross, D. 1988. Electromobile surface charge alters membrane potential changes induced by applied electric fields. *Biophys. J.* 54:879–884.

Gross, D., L. M. Loew, and W. W. Webb. 1986. Optical imaging of cell membrane potential changes induced by applied electric fields. *Biophys. J.* 50:339–348.

Hibino, M., H. Itoh, and K. Kinosita, Jr. 1993. Time courses of cell electroporation as revealed by submicrosecond imaging of transmembrane potential. *Biophys. J.* 64:1789–1800.

Hibino, M., H. Sighemori, H. Itoh, K. Nagayama, and K. Kinosita, Jr. 1991. Membrane conductance of an electroporated cell analyzed by submicrosecond imaging of transmembrane potential. *Biophys. J.* 59: 209–220.

Kinosita, K., Jr., I. Ashikawa, N. Saita, H. Yoshimura, H. Itoh, K. Nagayama, and A. Ikegami. 1988. Electroporation of cell membrane visualized under a pulsed-laser fluorescence microscope. *Biophys. J.* 53: 1015–1019.

Kinosita, K., Jr., M. Hibino, H. Itoh, M. Shigemori, K. Hirano, Y. Kirino, and T. Hayakawa. 1992. Events of membrane electroporation vizualized on a time scale from microsecond to second. *In* Guide to Electroporation and Electrofusion. D. C. Chang, B. M. Chassy, J. A. Saunders, and A. E. Sowers, editors. Academic Press, San Diego. 29–46.

Kinosita, K., Jr., H. Itoh, S. Ishiwata, K. Hirano, T. Nishizaka, and T. Hayakawa. 1991. Dual-view microscopy with a single camera: real-time imaging of molecular orientation and calcium. *J. Cell Biol.* 1:67–73.

Kinosita, K., Jr., and T. Y. Tsong. 1977. Voltage induced pore formation and hemolysis of human erythrocytes. *Biochim. Biophys. Acta.* 471: 227–242.

Marszalek, P., D. S. Liu, and T. Y. Tsong. 1990. Schwan equation and transmembrane potential induced by alternating electric field. *Biophys J.* 58:1053–1058.

Mehrle, W., U. Zimmermann, and R. Hampp. 1985. Evidence for asymetrical uptake of fluorescent dyes through electro-permeabilized membrane of *Avena* mesophyll protopast. *FEBS Lett.* 185:89–94.

Neumann, E. 1989. The relaxation hysteresis of membrane electroporation. *In* Electroporation and Electrofusion in Cell Biology. E. Neumann, A. E. Sowers, and C. A. Jordan, editors. Plenum, New York. 61–82.

Prausnitz, M. R., J. D. Corbett, J. A. Gimm, D. E. Golan, R. Langer, and J. C. Weaver. 1995. Millisecond measurement of transport during and after an electroporation pulse. *Biophys. J.* 68:1864–1870.

Robello, M., and A. Gliozzi. 1989. Conductance transition induced by an electric field in lipid bilayers. *Biochim. Biophys. Acta.* 982:173–176.

Rols, M. P., and J. Teissié. 1989. Ionic-strength modulation of ellectrically induced permeabilization and associated fusion of mammalian cells. *Eur. J. Biochem.* 179:109–115.

Rols, M. P., and J. Teissié. 1990. Electropermeabilization of mammalian cells. Quantitative analysis of the phenomenon. *Biophys. J.* 58: 1089–1098.

Rossignol, D. P., G. L. Decker, W. J. Lennarz, T. Y. Tsong, and J. Teissié. 1983. Induction of calcium-dependent, localized cortical granule breakdown in sea-urchin eggs by voltage pulsation. *Biochim. Biophys. Acta.* 763:346–355.

Sale, J. H., and W. A. Hamilton. 1968. Effects of high electric field on microorgnisms. III. Lysis of erythrocytes and protoplasts. *Biochim. Biophys. Acta.* 163:37–43.

Sator, V., M. A. Raftery, and M. Martinez-Carrion. 1977. Propidium as a probe of acetylcholine receptor binding sites. *Arch. Biochem. Biophys.* 184:95–102.

Schwister, K., and B. Deuticke. 1985. Formation and properties of aqueous leaks induced in human erythrocytes by electrical breakdown. *Biochim. Biophys. Acta.* 816:332–348.

Sixou, S., and J. Teissié. 1993. Exogenous uptake and release of molecules by electroloaded cells: a digitized videomicroscopy study. *Bioelectrochem. Bioenerg.* 31:237–257.

Sowers, A. E., and M. R. Lieber. 1986. Electropore diameters, lifetimes, numbers, and localization in individual erythrocyte ghost. *FEBS Lett.* 205:179–184.

Teissié, J., and M. P. Rols. 1993. An experimental evaluation of the critical potential difference inducing cell membrane electropermeabilization. *Biophys. J.* 65:409–413.

Teissié, J., and T. Y. Tsong. 1981. Electric field induced transient pores in phospholipid bilayer vesicles. *Biochemistry.* 20:1548–1554.

Tekle, E., R. D. Astumian, and P. B. Chock. 1990. Electro-permeabilization of cell membrane: effect of the resting membrane potential. *Biochem. Biophys. Res. Commun.* 172:282–287.

Tekle, E., R. D. Astumian, and P. B. Chock. 1991. Electroporation by using bipolar oscillating electric field: an improved method for DNA transfection of NIH 3T3 cells. *Proc. Natl. Acad. Sci. USA.* 88:4230–4234.

Tekle, E., R. D. Astumian, and P. B. Chock. 1994. Selective and asymetric molecular transport across electroporated cell membranes. *Proc. Natl. Acad. Sci. USA.* 91:11512–11516.

Tomov, T. C., and I. C. Tsoneva. 1989. Changes in the surface charge of cells induced by electrical pulses. *Bioelectrochem. Bioenerg.* 22: 127–133.

Zimmermann, U., and J. Vienken. 1984. Electric field-mediated cell-to-cell fusion. *In* Cell Fusion: Gene Transfer and Transformation. R. F. Beers and E. G. Bassett, editors. Raven Press, New York. 171–187.